Article:
Chen, X and Richter, RP (2019) Effect of calcium ions and pH on the morphology and mechanical properties of hyaluronan brushes. Interface Focus, 9 (2). 20180061. ISSN: 2042-8898

https://doi.org/10.1098/rsfs.2018.0061

Effect of calcium ions and pH on the morphology and mechanical properties of hyaluronan brushes

Xinyue Chen,[1,§] and Ralf P. Richter[1,2,*]

[1] *CIC biomaGUNE, San Sebastian, Spain*
[2] *School of Biomedical Sciences, Faculty of Biological Sciences, School of Physics and Astronomy, Faculty of Mathematics and Physical Sciences, and Astbury Centre of Structural Molecular Biology, University of Leeds, Leeds, United Kingdom*

[§] *Current address: Department of Physics and Astronomy, and Department of Oncology and Metabolism, University of Sheffield, Sheffield, United Kingdom*

* *Corresponding author: email r.richter@leeds.ac.uk*

ABSTRACT. Hyaluronan (HA) is a linear, regular polysaccharide that plays as a chief structural and functional component in peri- and extracellular matrices, thus contributing significantly to many basic cellular processes. To understand more comprehensively the response of the supramolecular organization of HA polymers to changes in their aqueous environment, we study the effects of Ca^{2+} concentration and pH on the morphology and viscoelasticity of films of end-grafted HA polymers on planar supports (HA brushes), as a well-defined in vitro model system of HA-rich matrices, by reflection interference contrast microscopy and quartz crystal microbalance. The thickness and softness of HA brushes decrease significantly with Ca^{2+} concentration, but do not change with pH, within the physiological ranges of these parameters. The effect of Ca^{2+} on HA brush thickness is virtually identical to the effect of Na^{+} at 10-fold higher concentrations. Moreover, the thickness and softness of HA brushes decreases appreciably upon HA protonation at pH < 6. Effects of pH and calcium ions are fully reversible over large parameter ranges. These findings are relevant for understanding the supramolecular organization and dynamics of HA-rich matrices in biological systems and will also benefit the rational design of synthetic HA-rich materials with tailored properties.

KEYWORDS. hyaluronan brush, viscoelasticity, thin film, QCM-D, RICM, pericellular coat

INTRODUCTION

As a chief component of extracellular matrix (ECM), hyaluronan (HA) is ubiquitous in the extracellular space of vertebrates and plays various biological roles. It is a linear, unbranched polysaccharide composed of identical disaccharide units containing glucuronic acid and N-acetylglucosamine.[1] Each disaccharide, which is 1.0 nm long,[2] carries one chargeable carboxylic group. The pK_a of polymeric HA is approximately 3, which implies that HA is negatively charged at physiological pH.[3]

Cells use HA synthases (HASs) in the plasma membrane to synthesise HA and extrude it into the extracellular space[4]. HA molecules produced can thus reach a very high molecular weight, up to millions of Daltons.[1] HA can either be released into the extracellular space, or remain grafted to the cell surface via HASs[4] or otherwise attached through HA receptors, such as CD44,[5] to form so-called pericellular coats (PCCs). HA-rich PCCs fulfil crucial functions in basic cellular processes such as proliferation and migration[6], intercellular adhesion,[7] and mechanosensing.[8] To modulate these functions, the morphology and physical properties of HA-rich PCCs are remodelled by changes in the extracellular environment. HA-binding proteins, for example, can induce condensation and rigidification (by cross-linking, such as with the inflammation-associated protein TSG-6[9]) or swelling of HA-rich matrices (by intercalation of swollen proteoglycans such as aggrecan[10,11]).[12] On a more basic level, the physico-chemical properties of the aqueous solution such as pH and ionic strength also affect the properties of HA and the assemblies that it forms. This is not only relevant for the function of HA-rich matrices around cells and in biological tissues, where changes in salt concentration and pH modulate HA-related functions.[13-16] Artificial HA-rich matrices[17] and surface coatings[18] have become popular in bioengineering research, and a good knowledge of the effect of pH and salts on the ultra-structure and mechanical properties of HA-rich matrices is thus also important for technological applications. Previous studies focussing on HA solutions have shown that besides monovalent cations such as sodium,[19,20] divalent calcium ions and pH also modulate the molecular structure and viscoelasticity of HA.[21-27] In biological and synthetic materials, however, HA is confined by cross-linking (in hydrogels) or by grafting or adsorption (in interfacial films), and there is still very limited information about the impact of environmental conditions such as pH and salts on such supramolecular HA assemblies.

Here, we study the effect of environmental conditions on films of HA polymers that are grafted via their reducing end to a planar support (Fig. 1*A*). These films are less complex than native PCCs yet they reproduce salient features such as the confinement of HA to a surface, the HA density in, and typical thickness of, PCCs. Moreover, they are well defined in that the molecular weight and arrangement of HA are tightly controlled. This enables quantitative studies and correlation with polymer physics theory that would not be possible with native PCCs. The repulsion between neighbouring HA chains induces their stretching away from the surface and films of end-grafted HA are adequately described as polyelectrolyte brushes. In previous work, we quantified the mechanical properties of such HA brushes at physiological ionic strength and pH,[28] and also how the monovalent salt NaCl affects HA brush morphology and mechanical properties.[29] These data revealed how the strong charge and the intrinsic stiffness of HA lead to brush properties that are distinct from those observed for synthetic polyelectrolytes. In the present study, we employ two surface-sensitive analysis techniques, reflection interference contrast microscopy (RICM) and quartz crystal microbalance with dissipation monitoring (QCM-D), to quantify the effects of calcium ions and pH on the thickness and softness of HA brushes systematically over an extensive parameter range, that is, calcium concentrations

between 1 µM and 1 M, and pH values between 1.0 and 9.0. The study sheds light on the effect of calcium and pH on the supramolecular organization and physical properties of surface-confined HA chains and highlights HA to be exquisitely responsive to these stimuli, both in terms of the magnitude and the reversibility of the response.

EXPERIMENTAL SECTION

Materials

The oligo-ethylene glycol (OEG) solution was a mixture of 99% of 1 mM OEG thiol (M_w 386.5 Da) and 1% of 1 mM biotinylated OEG thiol (788 Da; both from Polypure, Oslo, Norway) in synthesis grade ethanol, stored in the dark at 4 °C. Lyophilised streptavidin (SAv; 60 kDa; Sigma-Aldrich) was dissolved in ultrapure water. The stock solution at 1 mg/mL was stored as aliquots at -20 °C. Lyophilised hyaluronan, biotinylated at its reducing end (b-HA) and with well-defined molecular masses of 280 ± 14 kDa (Select-HA B250) and 58 ± 3 kDa (Select-HA B50), as well as nonbiotinylated HA of 237 ± 12 kDa (Select-HA 250), were from Hyalose (Oklahoma City, USA). HA was suspended in ultrapure water at 1 mg/mL (HA) or 0.5 mg/mL (b-HA), gently shaken at 4 °C for 2 h for reconstitution, and stored at -20 °C.

All buffer and salt solutions were prepared in ultrapure water (resistance 18.2 MΩ/cm), and degassed before use. The sample preparation buffer contained 10 mM HEPES and 150 mM NaCl at pH 7.4. NaCl and $CaCl_2 \cdot 2H_2O$ were from Sigma Aldrich. Potassium phosphate solutions with pH values ranging from 9.0 to 5.0 were prepared by mixing desired ratios of stock solutions, 100 mM KH_2PO_4 (Sigma Aldrich) and 50 mM K_2HPO_4 (Fluka, Germany), prior to use. The potassium phosphate solution with pH 5.0 was further titrated by concentrated HCl (37%, reagent grade; Scharlab, Spain) to obtain solutions with pH values down to 1.0.

Polystyrene microspheres with 23.7 ± 1.5 µm diameter (Polysciences, Hirschberg, Germany) were washed in ethanol and ultrapure water, and stored at 4 °C in ultrapure water.

Preparation of substrates

Glass cover slips (#1.5, 24 × 24 mm^2; Menzel Gläser, Germany) were gently wiped with lint-free tissue (Kimtech Science, Surrey, UK), blow-cleaned with N_2 gas, immersed in freshly prepared piranha solution composed of concentrated H_2SO_4 (95% to 98%) and H_2O_2 (50%; both Scharlab) at a volume ratio of 3:1 for 3 h, thoroughly rinsed with ultrapure water, blow-dried with N_2 gas and stored in sealed petri dishes. To obtain gold (Au) coated substrates, clean glass cover slips underwent 10 min plasma cleaning in the vacuum chamber of the magnetron sputter system (ATC 1800 UHV; AJA International, Scituate, MA) before deposition of an adhesive titanium (Ti; 0.5 nm) and a 5 nm Au layer. The layer thickness was determined from the deposition rate which was calibrated by spectroscopic ellipsometry on reference silicon wafers. Au-coated QCM-D sensors (QSX301; Biolin Scientific, Västra Frölunda, Sweden) were rinsed with ethanol and ultrapure water and blow-dried with N_2 gas. Prior to use, all substrates were UV-ozone treated (ProCleaner; Bioforce Nanoscience, Ames, IA) for 30 min.

Preparation of HA brushes

Cleaned gold-coated substrates were immersed in OEG solution overnight, rinsed with ethanol and ultrapure water, blow-dried with N_2 gas, installed in fluidic devices for QCM-D or RICM, and covered with sample preparation buffer. The surfaces were then sequentially exposed to SAv (20 µg/mL; 30 min) and b-HA (5 µg/mL for QCM-D, 20 µg/mL for RICM; 2 h) in

sample preparation buffer, with each incubation step followed by abundant rinsing to remove excess molecules from the solution phase.

Quartz crystal microbalance with dissipation monitoring

QCM-D measurements were performed with a QSense E4 system (Biolin Scientific) in flow mode (5 to 20 µL/min, adjusted with a syringe pump; KD Scientific, Holliston, MA) at a working temperature of 24 °C on Au-coated QCM-D sensors with an OEG monolayer. Changes in the sensor resonance frequency (Δf_i) and dissipation (ΔD_i) were collected at 6 overtones (i = 3, 5, 7, 9, 11, 13, corresponding to resonance frequencies of $f_i \approx$ 15, 25, 35, 45, 55, 65 MHz); for simplicity, only selected overtones (i = 3, 7, 11) are presented. As controls, measurements were also performed on surfaces covered by SAv, with or without 10 µg/mL of non-biotinylated HA in the ambient solution.

Reflection interference contrast microscopy

For RICM, we used fluidic chambers in the form of cylindrical open cuvettes (5 mm diameter) made from a tailored Teflon holder and a glass cover slip at the bottom, glued together with two-component glue (Twinsil; Picodent, Germany). Cuvettes were used with a liquid volume of 50 µL. Samples were injected and the solution was rapidly homogenised with a pipette. Excess molecules were removed from the solution phase by repeated dilution and aspiration of the cuvette content until a concentration reduction of at least 10^5 fold was reached. Care was taken to keep the glass cover slip wet throughout all solution exchanges. A separate cuvette was used to test for the effect of each salt ($CaCl_2$ or NaCl) concentration or pH on HA brush thickness. Polystyrene microspheres for RICM analysis were added 15 min after incubation of a given test solution.

Interferographs were obtained with an inverted microscope (Axio Observer Z1; Zeiss, Oberkochen, Germany) in epi-illumination reflection mode, using a XBO xenon short-arc lamp as light source, an antiflex oil immersion objective (EC Plan Neofluar Antiflex 63×/1.25; Zeiss) and a filter cube with two crossed polarisers (AHF Analysentechnik, Germany).[30] The reflected light passed through a custom-built beam splitter unit[28] with band pass filters which in combination with two CCD cameras (ORCA-ER; Hamamatsu Photonics, France) permitted simultaneous acquisition of interferographs at wavelengths λ = 630 nm, 546 nm and 490 nm. The opening of the aperture diaphragm was reduced to its minimum throughout all measurements.

To quantify the distance between the polystyrene sphere and the substrate surface, we adapted a previously established algorithm implemented in Matlab.[28] Briefly, the method is based on the determination of the position of extrema in the radial intensity profile of interferographs,[30] and has an estimated accuracy of ± 5 nm. The method was here adapted to account for the presence of the metallic coating and the OEG and SAv layers (see Supplementary Methods and Fig. S1). 10 polystyrene beads were analyzed per sample, and mean distances ± standard deviation were used for further analysis.

RESULTS

Assembly of HA brushes

Hyaluronan brushes were formed, as schematically shown in Fig. 1*A*, by grafting of HA with well-defined molecular weight (280 ± 14 kDa) via a biotin at the reducing end to a monolayer of streptavidin supported by a biotinylated thiol-OEG-monolayer on gold. This approach has been

established previously.[9,31] QCM-D was used to follow the main assembly steps (Fig. 1*B*). To a first approximation, a decrease in frequency shift Δf indicates an increase in the surface-bound mass (including hydrodynamically coupled water), whereas the dissipation shift ΔD reflects the softness of the surface-associated film.[31]

The frequency and dissipation shifts upon SAv injection (Fig. 1*B*, 40 to 70 min; final shifts $\Delta f_3/3 = -24 \pm 1$ Hz and $\Delta D_3 = 0.2 \pm 0.2\ 10^{-6}$) were in good agreement with previous studies,[9] and confirm the formation of a dense and stably anchored SAv monolayer. Subsequent incubation with biotinylated HA (Fig. 1*B*, 90 to 210 min) led to an additional decrease in the normalised frequency shift ($\Delta f_3/3 = -9 \pm 1$ Hz) and a large increase in dissipation ($\Delta D_3 = 9 \pm 1 \times 10^{-6}$). The latter observation, together with significant spreading of the responses between different overtones, is consistent with the formation of a highly hydrated and soft film, as expected for HA brushes.[10] The rate of frequency and dissipation changes gradually decreased with progressing b-HA incubation time and virtually stabilised after 2 h; these responses are consistent with the formation of a polyelectrolyte brush, where the HA film increasingly hampers penetration and surface-binding of new molecules as it becomes denser. HA molecules were also stably grafted as demonstrated by the lack of response upon rinsing with buffer (Fig. 1*B*; >210 min).

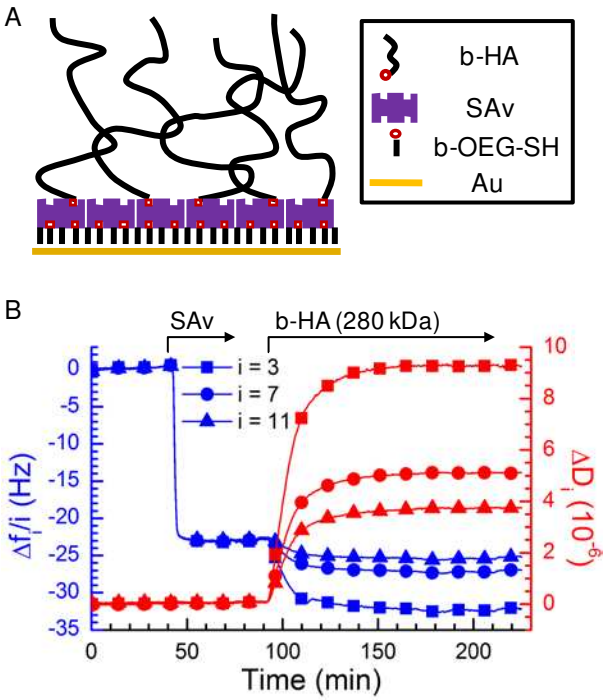

Figure 1. (*A*) Schematic of the build up of HA brushes (not to scale). (*B*) Assembly of an HA brush; a biotinylated OEG monolayer on gold was formed *ex situ* and all subsequent assembly steps were followed by QCM-D. Normalised frequency shifts ($\Delta f_i/i$) and dissipation shifts (ΔD_i) at overtones i = 3, 7, 11 are presented. The start and duration of incubation of each sample (20 µg/mL SAv and 5 µg/mL b-HA) are indicated by arrows on top; during remaining times, the surface was exposed to sample preparation buffer (10 mM HEPES, 150 mM NaCl, pH 7.4).

HA film thickness, response to NaCl, and grafting density

Colloidal probe RICM was used to quantify the thickness of the HA film. The method measures the distance between a colloidal sphere and a planar transparent substrate,[30] with a

resolution of a few nanometers by the analysis of interference patterns arising from partial reflection of light at the interfaces between the planar SAv-covered substrate and the solution, and between the solution and the colloidal probe. Analogous to previous work by us and others,[31,32] we used triple wavelength RICM to unambiguously resolve the thickness over a range of 1 µm, but we here refined the analysis method to account for the presence of the semi-transparent gold coating and the OEG and SAv layers (see Supplementary Methods and Fig. S1).

The mean thickness of the HA film in sample preparation buffer (containing 150 mM NaCl and pH 7.4, close to physiological ionic strength and pH) was 207 nm. The standard deviation across 10 colloidal probes randomly positioned on the same surface was typically ± 10 nm, and the standard deviation of the mean values of 5 measurements on independently prepared HA films was ± 5 nm. This demonstrates that the HA brushes are laterally homogeneous and that their preparation is reproducible. With a contour length of 1.0 nm per disaccharide[2] and a molecular mass of 378 Da per disaccharide, the contour length of 280 ± 14 kDa HA is l_c = 740 ± 37 nm, and at physiological ionic strength and pH, an unperturbed HA chain of this length is expected to form a random coil with a radius of gyration of $R_g \approx 40$ nm.[33] The HA chains are thus significantly stretched compared to their dimensions in solution, confirming that a polyelectrolyte brush is effectively formed.

To further validate the integrity of the HA brush, we quantified the brush thickness as a function of NaCl concentration. We have previously reported a detailed analysis of such a dependence for brushes of HA with a distinct molecular weight (1083 kDa),[29] which serves as a benchmark for the present work. The distance *H* between polystyrene spheres floating on the HA brush and the SAv-coated substrate was again used as an approximate measure of the brush thickness, and the results are shown in Fig. 2*A* (*red line with solid circles*). Consistent with our previous findings,[29] *H* decreased monotonically with increasing NaCl concentration. The shape of the curve was qualitatively consistent with theoretical predictions for brushes of strongly charged polyelectrolytes.[34-36] Specifically, at low ionic strength ([NaCl] ≤ 0.5 mM) the measured thickness varied only weakly, and this regime corresponds to the 'osmotic brush' regime[35] where the brush thickness is determined by the balance of the osmotic pressure of counterions trapped in the brush and the entropy of chain stretching.[34] At higher ionic strengths (1 mM ≤ [NaCl] ≤ 1000 mM), salt screens the electrostatic interactions ('salted brush' regime)[35] and leads to a progressive decrease in brush thickness. At very high ionic strength, it is expected that the screening becomes so strong that the excluded volume repulsion of the uncharged polymer backbone (intrinsic excluded volume) dominates the brush behaviour and the dependence on ionic strength again weakens. This 'quasi-neutral' brush regime is barely reached in the experiment presented here. We note that the slope for the salted brush regime in the log-log plot is -0.22, which deviates from the power of -1/3 expected by simple theory.[34-36] We had previously demonstrated that the apparent attenuation of the salt dependence compared to the theoretical prediction is expected and due to two distinct effects:[29] towards low ionic strength, HA brushes become strongly stretched (with H/l_c larger than 0.5) and the resistance to stretching thus becomes stronger than what is predicted according to the Gaussian chain approximation used in the theory; towards high ionic strength, on the other hand, the intrinsic excluded volume of the uncharged polymer backbone, which is positive for HA but not considered in the scaling theory, increasingly contributes to inter-chain repulsion and thus limits the screening effect of the salt.

In our previous work, we also showed that the combined effect of intrinsic excluded volume and electrostatic repulsion on HA brush morphology can be quantitatively reproduced in the limit of high ionic strength (NaCl $\geq$ 50 mM) with an analytical self-consistent mean-field theory.[29] With this approach, we can estimate the grafting density of the HA brush studied here (Fig. S2), and the root-mean-square (rms) distance between anchor points is $s \approx 50$ nm. From the HA molecular weight, the brush thickness and the grafting density, one can estimate the concentration of chargeable groups in the HA brush to match the concentration of added salt at around 0.8 mM NaCl. This value is consistent with the transition between the osmotic and salted brush regimes identified above.

Detailed inspection of the bead-substrate distances H in Fig. 2*A* reveals that these exceed the contour length of the HA chain without added salt or at very low NaCl concentrations. Specifically, in ultrapure water, H exceeded l_c by approximately 220 nm. This result was unexpected and was not observed in the earlier study with HA brushes made from approximately 4 times larger HA chains.[29] On the other hand, we found the bead-substrate distance on HA brushes made from smaller HA chains (58 ± 3 kDa) to be 579 ± 8 nm in ultrapure water, that is, the discrepancy with the contour length (153 ± 8 nm) is even larger than in the case of 280 kDa b-HA. Clearly, the polystyrene bead hovers at a certain distance above the HA brush and we propose that this is due to repulsive electrostatic interactions between the negatively charged polystyrene bead and an excess negative charge displayed by the HA brush. The grafting density of the HA brush is expected to increase with decreasing HA size in our assays, because the kinetic limitations associated with brush formation become less severe for shorter chains.[37] The stretching of the HA chains and also the excess charge of the brush[29] would increase with grafting density, and the thickness trends as a function of HA molecular weight would thus be consistent with such a scenario.

Our finding thus indicates that H can significantly overestimate the brush thickness in the limit of low ionic strength. A quantitative estimation of the magnitude of the discrepancy appears difficult, because we lack the surface charge density on the colloidal sphere. However, with increasing salt concentration, the charges are screened, and we thus expect that the error is progressively decreasing as salt is added. At the same time, the colloidal probe will exert some pressure on the brush due to gravitation and H may thus effectively underestimate the thickness of the unperturbed brush. However, the forces acting on the brushes are small, less than 4 pN considering that gravitational forces are offset by buoyancy, and we thus estimate this effect to be small.[29]

Impact of calcium ions on HA films

Morphology

We used colloidal probe RICM to analyze the impact of $CaCl_2$ on HA film thickness (Fig. 2*A*, *black line with squares*). As for NaCl, the HA film thickness decreased monotonically with increasing $CaCl_2$ concentration, with the salt dependence being most pronounced at intermediate $CaCl_2$ concentrations (0.1 mM $\leq$ [$CaCl_2$] $\leq$ 100 mM) and a trend towards plateaus at higher and lower $CaCl_2$ concentrations. Over the entire range of $CaCl_2$ concentrations, the film thickness was reproducible to within a few nanometres across the measured surfaces, and the film thickness remained well above the rms distance between grafting points. Thus, the HA polymers retain their hydrated and stretched, homogeneous brush conformation even at the highest $CaCl_2$ concentration.

Closer inspection revealed a high degree of similarity in the responses of HA brushes to the two salts. The curves for $CaCl_2$ and NaCl could be virtually overlaid on a single master curve through a simple re-scaling of the $CaCl_2$ concentration by a factor of 10 (Fig. 2*B*). This indicates that the effect of calcium ions on the interaction between HA chains in the brush, and apparently also the repulsion between the HA brush and the colloidal probe in the limit of low ion concentrations, is equivalent to the effect of sodium ions at 10-fold higher concentration. Such a simple scaling is remarkable, considering that the two cations have different valency and that the dependence of brush thickness on ion concentration is rather complex. Moreover, the scaling factor of 10 is substantially larger than what would be predicted for simple charge screening: the ionic strength, defined as $I = 1/2 \sum_i z_i^2 c_i$ where c_i are the molar concentrations of ions of valency z_i, is increased by 3-fold for $CaCl_2$ as compared to NaCl at the same molar cation concentration. This comparison implies that the simple scaling by a factor 10 must arise from a combination of several distinct effects, which we shall discuss later (vide infra).

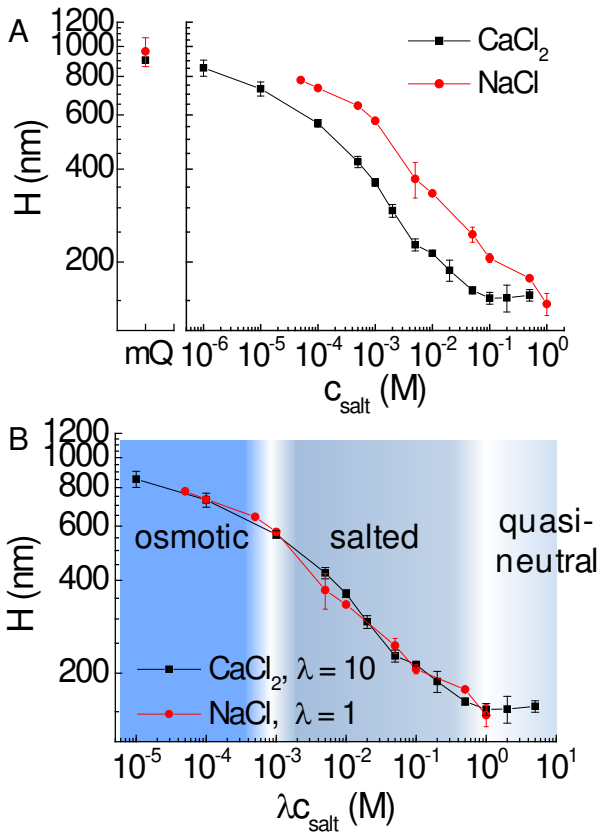

Figure 2. Effect of sodium and calcium ions on HA brush thickness. (*A*) The distance *H* of colloidal probes (polystyrene beads, around 24 µm diameter, hovering on top of HA brushes due to gravitation) from the SAv-coated substrate was quantified by RICM and is a measure of the HA film thickness. HA brushes were prepared as shown in Fig. 1*B*, and data represent means and standard deviations from two independent experiments. Next to $CaCl_2$ (*black squares*), results for NaCl (*red circles*) are also shown, together with results in ultrapure water without added salt (mQ). (*B*) Both data sets superpose when the salt concentration is re-scaled, by multiplication with $\lambda = 1$ for NaCl and $\lambda = 10$ for $CaCl_2$. The three canonical brush regimes – osmotic, salted and quasi-neutral – can be identified and are indicated with the coloured background.

Visco-elastic properties

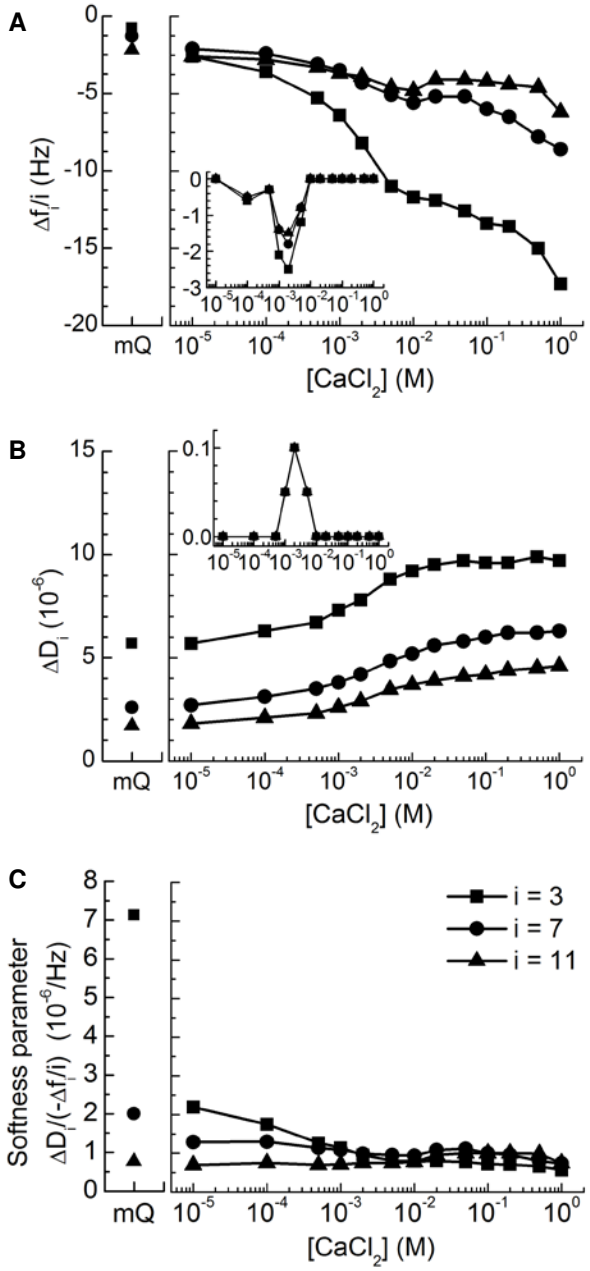

Figure 3. Effect of calcium ions on HA brush rigidity, characterised by QCM-D. Normalised frequency shifts ($\Delta f_i/i$; *A*), dissipation shifts (ΔD_i; *B*) and softness parameter ($\Delta D_i/(-\Delta f_i/i)$; *C*) are displayed for selected overtones (i = 3, 7 and 11, as indicated in *C*). HA brushes were prepared as in Fig. 1*B*, and data represent responses at equilibrium of the HA film compared to a reference SAv monolayer film as a function of the $CaCl_2$ concentration in ultrapure water (see Fig. S3 for details; data in ultrapure water without added salt are also shown, as mQ). Responses upon exposure of non-biotinylated HA (10 µg/mL) to the SAv monolayer are shown for comparison in the *insets* in *A* and *B*; these show minor non-specific binding at intermediate $CaCl_2$ concentrations and correlate with transient minima in the frequency shifts for the HA brush. The softness parameter indicates HA brush stiffening with $CaCl_2$ concentration.

The effect of Ca^{2+} on the visco-elastic properties of HA brushes was characterised by QCM-D. To this end, frequency and dissipation shifts upon variation of the ambient $CaCl_2$ concentration were monitored on HA brushes (Fig. S3*A*) as well as reference surfaces (bare SAv without HA; Fig. S3*B*). By subtracting the responses on the reference surfaces from those on the HA brushes, the effect of the HA brush could be discriminated from the effects of the ions on the density and viscosity of the solution phase, to which the QCM-D is also sensitive. These data are shown in Fig. 3*A*-*B*. In addition, we also examined over the full range of $CaCl_2$ concentrations if non-biotinylated HA polymers (237 ± 12 kDa, at 10 µg/mL) bind to the reference surface (Fig. S3*C*), and these effects are shown as insets in Fig. 3*A*-*B*. Fig. 3*C* shows the ratio of dissipation and frequency shifts $\Delta D_i/(-\Delta f_i/i)$. This parameter is related to the mechanical properties of the surface-confined films: for very thin films, it is proportional to the elastic compliance, a measure of film softness.[39] The HA films studied here are too thick for this proportionality to hold, and the parameter should thus be considered an effective and relative measure of HA brush softness.

Overall, the film softness decreased with increasing calcium concentration, a trend that is expected as the salt-induced contraction of the HA brush (Fig. 2) makes the film denser. The dependence is monotonous except for a shallow local minimum around 2 mM $CaCl_2$. At this salt concentration, we also found HA to show minor yet significant non-specific interaction with the SAv substrate which was not present at lower and higher $CaCl_2$ concentrations (Fig. 3*A*, *inset*). The local minimum in the softness parameter, therefore, most likely is the consequence of a slight perturbation of the HA brush morphology by binding of a fraction of the HA chains to the SAv substrate in addition to the biotin anchorage. It is also notable that the softness parameter (Fig. 3*C*) does not show the pronounced sigmoidal dependence on the calcium concentration that we had observed for the HA brush thickness (Fig. 2). In particular, the rapid decrease in softness in the low calcium concentration regime (osmotic brush) suggests that the mechanical properties of the HA brush are sensitive to calcium concentration in the osmotic brush regime even though the thickness remains roughly unchanged.

We also note that the effect of calcium on the HA brushes was fully reversible for most of the calcium concentrations investigated, that is, QCM-D responses in ultrapure water before and after exposure to each calcium concentration were comparable (Fig. S3*A*). Exceptions in this regard were the highest calcium concentrations (≥ 100 mM), for which a fraction of the frequency and dissipation shifts was not recovered upon rinsing in ultrapure water, as shown in detail in Fig. S4. Apparently, very high calcium concentrations can promote irreversible (though minor) changes to the HA brush.

Impact of pH on HA films

Morphology

The effect of pH on the thickness of HA brushes was again characterised by RICM (Fig. 4*A*). We used potassium phosphate as buffering agent throughout, to avoid any effects due to variations in cation species or concentration. Phosphate buffer has pK_a values of 2.1, 7.2 and 12.3,[40] and we found the buffering capacity at a concentration of 100 mM K^+ to be satisfactory over the tested pH range (1.0 to 9.0).

Over a broad range around neutral pH ($6.0 \leq pH \leq 9.0$), *H* remained virtually constant at 216 ± 7 nm. This value matches the results for 100 mM NaCl (206 ± 7 nm; Fig. 2), indicating that potassium and sodium have very similar effects on the HA brush. The mean *H* decreased by

roughly two-fold between pH 6.0 to pH 3.0, and then remained roughly constant down to pH 1.0. The carboxyl groups in HA have a pK_a around 3,[3] and the reduction in film thickness is thus likely due to the protonation of carboxyl groups and loss of the polyelectrolyte character of the HA chains.

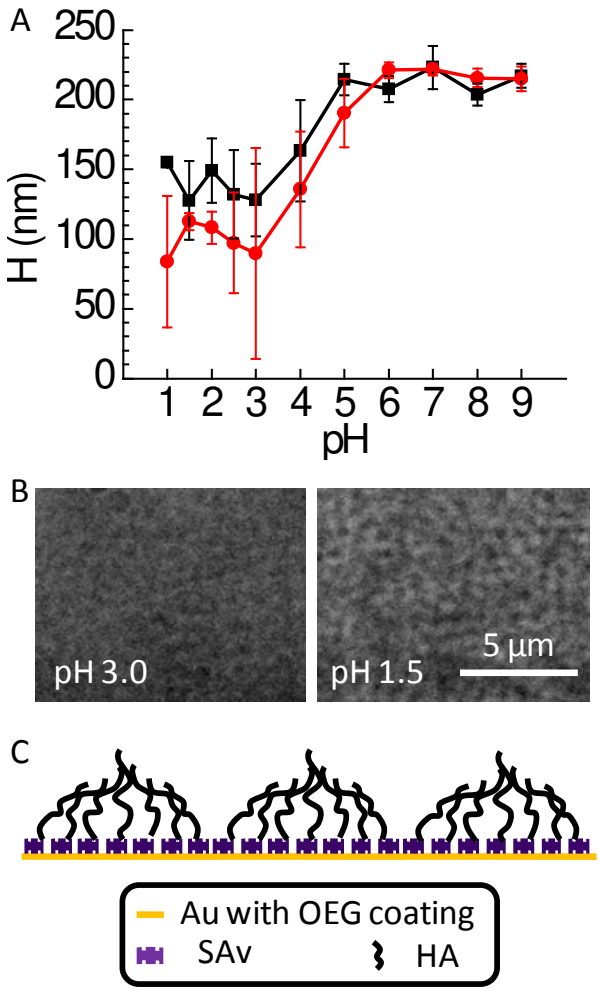

Figure 4. (*A*) Effect of pH on HA film thickness, quantified by RICM analogous to Fig. 2. Two independent experiments are shown. (*B*) Representative interferographs (w/o colloidal probe) of an HA film in the presence of pH 3 (*left*) and pH 1.5 (*right*). Interferographs at pH 1.5 reveal a distinctive pattern, that is not (or only faintly) visible at pH ≥ 3. The contrast of both images was adjusted consistently, and interferographs acquired at pH > 3 were comparable to what is shown here for pH 3. (*C*) Schematic of the hypothesised microphase formation in end-grafted HA films at low pH (not to scale).

It is notable that the standard deviations in *H* increased markedly at pH values ≤ 5 (Fig. 4*A*). This indicates that the HA film loses its homogeneity under strongly acidic conditions, and instead forms a film that is heterogeneous on the microscale. Circumstantial evidence for microscale heterogeneities also comes from interferographs taken on HA films in the absence of a colloidal probe. These revealed a distinctive pattern at pH 1.5 that was not (or only faintly) visible at pH values larger than 3 (Fig. 4*B*). The contrast and spatial resolution of the

interferographs are too low to assign a specific structure. However, the fact that we observe heterogeneities indicates that protonated HA becomes sticky, and we tentatively propose that the patterns arise from the clustering of sticky HA polymers into microdomains as schematically indicated in Fig. 4*C*. The formation of microphases is indeed predicted by theory[41,42] and was experimentally observed for brushes of cross-linked HA[12] and other polymers.[43]

Visco-elastic properties

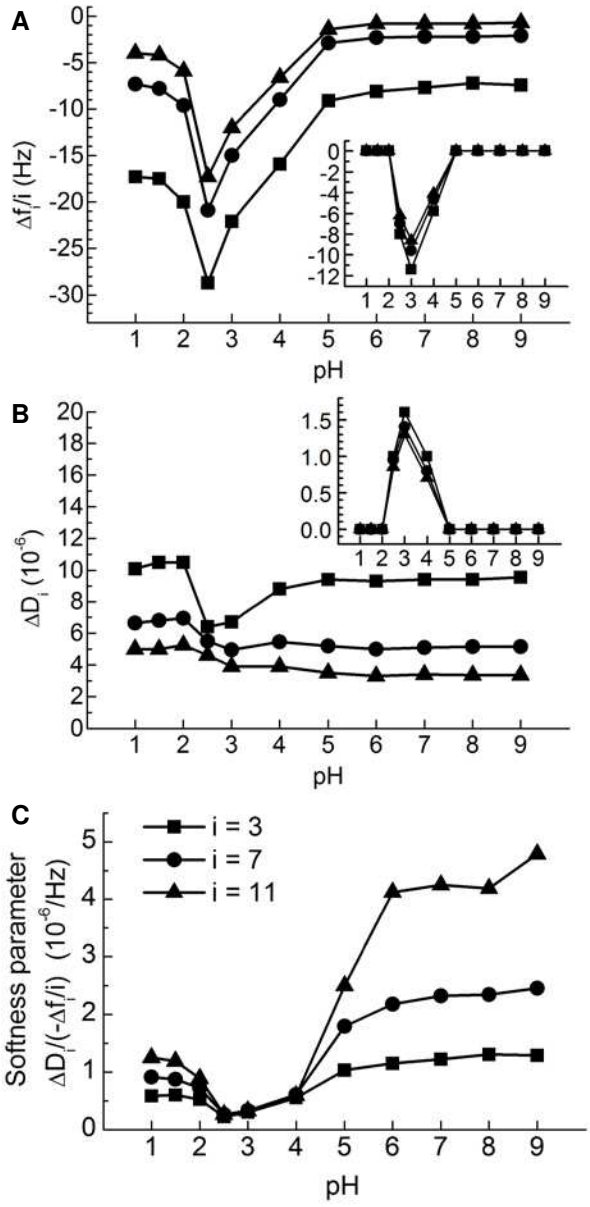

Figure 5. Effect of pH on HA brush rigidity, characterised by QCM-D. Data are displayed analogous to Fig. 3, in potassium phosphate buffer (containing 100 mM potassium) at various pH. The *insets* in *A* and *B* show strong non-specific binding of non-biotinylated HA at pH 4.0, 3.0 and 2.5. The softness parameter indicates that HA brush stiffening is most pronounced at these pH values.

QCM-D was again used to study the influence of pH on HA film softness (Figs. S5 and 5) following the method used for the characterization of the effect of $CaCl_2$ solutions (Figs. S3 and 3). The softness parameter (Fig. 5*C*) was not sensitive to pH between pH 6.0 and 9.0, but decreased substantially at lower pH values. The most rigid films (i.e. with the smallest softness parameter) occurred at pH 2.5. Below this pH value the HA films became again somewhat softer but clearly remained more rigid than at neutral pH. The effect of pH changes on HA brushes was fully reversible over the large range of pH variations studied, indicating that pH can be used for the reversible switching of HA brush properties. Notably, we did not find any indications for the degradation of HA upon exposure to pH down to 1.0, in contrast to some earlier reports studying HA in the solution phase.[26,27,44]

It is notable that HA polymers also showed rather strong non-specific binding to the SAv-coated substrate for pH values ranging between 2.5 and 4.0, whereas no such binding was detectable at lower and higher pH values (Fig. 5*A*-*B*, *insets*). The electrostatic potential of SAv is positive below pH 6,[45] and attractive electrostatic interactions between the (partially) de-protonated HA and the acidic SAv may well be responsible for the selective non-specific binding of HA between pH 2.5 and 4.0. Moreover, it is likely that the transient minimum in the softness parameter at pH 2.5 arises from a combination of inter-HA-chain attraction (after HA protonation) and HA-substrate attraction, whereas the values measured at pH 1.0 and 1.5 may well represent the genuine softness of the fully protonated HA brush (in the absence of attractive HA-substrate interactions).

DISCUSSION

On the qualitative level, the results of our systematic analysis of the response of HA brushes to calcium ions and pH are in line with the known properties of HA in the solution phase. In particular, the response of HA brushes to sodium and calcium ions (Fig. 2) confirms that HA around neutral pH behaves as a strongly charged and semi-flexible polyelectrolyte in good solvent (we here refer to semi-flexible as the statistical polymer segment length being much larger than the size of the chemical monomer). Moreover, a 'putty' gel state has been reported for HA solutions around pH 2.5,[26,46,47] and the collapse of HA brushes at low pH (Fig. 4*A*), accompanied by microphase formation (Fig. 4*B*-*C*) and film rigidification (Fig. 5), would be consistent with a transition from repulsive to attractive inter- and intra-chain interactions upon HA protonation.

On the quantitative level, a striking observation that to the best of our knowledge has not previously been reported is that divalent calcium ions affect the HA brush thickness in much the same way as monovalent sodium ions do at 10-fold higher concentrations. Can we explain such a similar behaviour? It is well known that divalent ions are more effective than monovalent ions in screening electrostatic interactions. However, this effect can only account for a 3-fold potentiation. We propose that calcium ions affect the measured brush thickness (Fig. 2*B*) by several distinct mechanisms that come into play in the different brush regimes.

Osmotic brush regimes (low calcium concentrations). For a polyelectrolyte brush in the osmotic regime, the brush morphology has been predicted to be sensitive to the valency of added ions:[48] ions with multiple charges can substitute several monovalent ions, thus reducing the number of mobile counterions that is necessary to compensate the polymer charge within the brush and thereby diminishing the osmotic pressure of the counterion gas. Specifically, with calcium and sodium having valencies of $z_{Ca} = 2$ and $z_{Na} = 1$, respectively, the brush thickness

would be expected to decrease by a factor of $\sqrt{z_{Ca}/z_{Na}} \approx 1.4$ for divalent counterions compared to monovalent counterions at the same molar ion concentration.[49] Our experimental data at 0.1 mM and 0.5 mM added salt showed a decrease in *H* by 1.3 and 1.5, respectively, which is in reasonably good agreement with the theoretical prediction. In addition, divalent counterions can decrease the surface potential more dramatically compared to monovalent ions,[38] or may even decrease the surface charge more effectively by counterion condensation. This would result in a decrease in the electrostatic repulsion between the HA brush and the surface of the polystyrene bead, which we have seen to be important at low ionic strength.

Salted and quasi-neutral brush regimes (high calcium concentrations). The thickness of a polyelectrolyte brush is expected to scale with the Debye screening length κ^{-1} as $H \sim \kappa^{-2/3}$ in the salted regime if the thickness changes were solely driven by electrostatic screening by free ions in the solution phase.[49] The Debye length scales as $\kappa^{-1} \sim 0.304\sqrt{[NaCl]}$ and as $\kappa^{-1} \sim 0.176\sqrt{[CaCl_2]}$,[38] and consequently, a reduction in thickness by a factor of $(0.304/0.176)^{2/3} \approx 1.4$ would be expected when replacing NaCl by $CaCl_2$ at a given salt concentration. Inspection of Fig. 2*A* reveals that the factor is significantly larger in our experiments (1.6 ± 0.1 between 1 and 50 mM salt). This is equivalent to our earlier statement that the 3-fold increased potency of $CaCl_2$ to screen electrostatic interactions is much smaller than the 10-fold potentiation observed in our experiments. Several additional mechanisms may play a role in enhancing the potency of $CaCl_2$. First, the polymer charge may be reduced due to condensation of calcium ions on the HA chains.[50] For polymers with monovalent charges such as HA, Manning theory[51] predicts partial condensation of counterions if the distance between charges on the polymer is smaller than $z\lambda_B$, where z is the counterion valency and λ_B = 0.71 nm the Bjerrum length. The distance of carboxyl groups on HA is 1.0 nm, implying that partial condensation is likely to ensue for calcium but not for sodium ions. Second, calcium ions may potentially also bridge carboxylic groups on HA owing to the bivalency of the calcium ions.[50] However, the stability (i.e. homogeneity and solvation) of the brush at very high calcium concentrations as observed here (Fig. 2), and the stability (i.e. lack of precipitation) of HA solutions at very high calcium concentrations observed by others,[19] suggest that such a cross-linking effect would be rather weak. Third, calcium may reduce the intrinsic stiffness of HA. This has indeed been suggested in previous works[23,52] although the magnitude of this effect has not been quantified to our knowledge. The thickness of a polymer brush scales with the intrinsic stiffness of the polymer p as $H \sim p^{1/3}$.[29] A decrease in intrinsic stiffness (or equivalently, the polymer´s persistence length) by 32% would hence be required to produce a thickness change by a factor $1.4/1.6 \approx 0.88$, if the intrinsic stiffness alone was to account for the impact of calcium on brush thickness beyond what is achieved by simple electroststic screening. Obviously, the above described mechanisms may also act together, to different extents depending on the calcium concentration.

Taken together, the mechanisms underlying the 10-fold potentiation of calcium over sodium ions with regard to brush thickness variations remains to be further elucidated. Future comparative studies with different divalent ions, and possibly also monovalent and trivalent ions, may help resolving this question. It will here also be interesting to quantify the intrinsic stiffness of HA chains as a function of ion concentration and type, for example, by single chain stretching experiments.[53]

The results of the present study are relevant for rationalizing the basic physical properties of HA-rich matrices in biological systems. We learn that protonation of carboxyl groups affects HA brush morphology and mechanical properties only at pH values below 6.0 and is thus unlikely to be relevant under physiological conditions. Electrostatic screening, on the other hand, has a dramatic effect on HA brushes. This effect is exerted by all free ions, although with a three-fold higher potency by $CaCl_2$ as compared to NaCl. The concentration of calcium ions in the extracellular space is on the order of 1 mM,[54] and thus more than 100-fold lower than the physiological concentration of the monovalent ions (mostly Na^+ and to a much lesser extent K^+). Therefore, sodium ions will account for most of the electrostatic screening whilst the contribution of calcium ions is rather marginal, on the order of a few percent. As discussed above, calcium clearly exerts effects additional to the electrostatic screening. In the future, it will be interesting to explore how important these additional effects are if the relatively low physiological calcium concentration is combined with the much higher physiological sodium concentrations. Naturally, the situation in native HA-rich matrices will be even more complex, for example, because HA-binding and other proteins also contribute to defining matrix assembly and dynamic reorganization, and their function may also be modulated by calcium ions. However, the simplified yet well-defined model system studied here provides an idea of the magnitude of effects that can occur and provides a reference for studies with more complex systems. Future studies should also consider if HA brushes respond in specific ways to other divalent ions (e.g. Mg^{2+} and Zn^{2+}). Work with HA solutions has proposed, for instance, that zinc(II) ions coordinate with HA,[55] and that copper(II) chloride may degrade HA,[56] and it will be interesting to see if such effects can also be observed in HA brushes.

Our results also provide information that should be useful for the rational design of HA-based materials with tailored properties. Here, HA brushes appear particularly attractive for the development of stimuli-responsive surface coatings: they combine a large dynamic range – such as a fivefold thickness change in response to ions (Fig. 2) and a twofold thickness change in response to pH (Fig. 4) – with a high degree of reversibility in the morphological changes, thus allowing for strong and repeatable switching by external stimuli. Changes in thickness can be exploited directly as a readout, or as a mechanical actuator, for sensing applications. Associated changes in brush concentration and hence physical properties such as viscoelasticity (Figs. 3C and 5C) or permeability could also be exploited for applications. An important parameter defining permeability is the correlation length ξ, a statistical measure of the distance between segments on neighbouring chains.[57] In homogeneous meshworks of flexible polymers, the correlation length is an effective measure for the mesh size, and in good solvent it is predicted to decrease with polymer concentration c with a power of -3/4.[58] For a given HA brush (i.e. at constant grafting density), we have thus $\xi \sim c^{-3/4} \sim H^{-3/4}$ to a first approximation, and a fivefold reduction in brush thickness would thus entail a more than threefold reduction in the size of particles that can effectively permeate the HA film.

CONCLUSIONS

In this work, we have systematically analyzed the variations in thickness (by colloidal probe RICM) and softness (by QCM-D) of HA brushes over a broad range of Ca^{2+} concentrations and pH. Within the physiologically relevant ranges of these two parameters, we found the softness and thickness of HA brushes to be exquisitely sensitive to Ca^{2+} concentrations but essentially insensitive to pH. More broadly, we discovered that the effect of divalent calcium ions on HA brush thickness is virtually identical to the effect of monovalent sodium ions at 10-fold higher

concentrations, and that HA brushes collapse upon protonation below pH 6.0. These findings are relevant for understanding the supramolecular organization and dynamics of HA-rich extracellular matrices and for the design of stimuli-responsive surface coatings with tailored properties.

DATA AND SUPPLEMENTARY MATERIAL

The supplementary material contains Supplementary Methods and Figures S1-5. Figures S3-5 represent datasets supporting this article.

AUTHOR CONTRIBUTIONS

RPR conceived the study; XC and RPR designed the experiments; XC performed the experiments; XC and RPR analyzed the data, and wrote the manuscript. All authors gave final approval for publication.

ACKNOWLEDGEMENTS

We thank Luis Yate (CIC biomaGUNE) for the preparation of gold-coated substrates, and Oleg Borisov (University of Pau, France) for fruitful discussions.

FUNDING SOURCES

This work was supported by the European Research Council (Starting Grant 'JELLY', FP7-ERC-2012-StG-306435 to R.P.R.), the Spanish Ministry for Economy and Competitiveness (MAT2014-54867-R to R.P.R) and the UK Biotechnology and Biological Sciences Research Council (BB/R000174/1 to R.P.R.).

COMPETING INTERESTS

We have no competing interests.

REFERENCES

(1) Fraser, J. R.; Laurent, T. C.; Laurent, U. B. Hyaluronan: its nature, distribution, functions and turnover. *J. Intern. Med.* **1997**, *242*, 27-33.

(2) Almond, A.; Brass, A.; Sheehan, J. K. Oligosaccharides as model systems for understanding water−biopolymer interaction: Hydrated dynamics of a hyaluronan decamer. *J. Phys. Chem. B* **2000**, *104*, 5634-40.

(3) Cleland, R. L.; Wang, J. L.; Detweiler, D. M. Polyelectrolyte properties of sodium hyaluronate. 2. Potentiometric titration of hyaluronic acid. *Macromolecules* **1982**, *15*, 386-95.

(4) Weigel, P. H.; Hascall, V. C.; Tammi, M. Hyaluronan synthases. *J. Biol. Chem.* **1997**, *272*, 13997-4000.

(5) Wolny, P. M.; Banerji, S.; Gounou, C.; Brisson, A. R.; Day, A. J.; Jackson, D. G.; Richter, R. P. Analysis of CD44-hyaluronan interactions in an artificial membrane system: insights into the distinct binding properties of high and low molecular weight hyaluronan. *J. Biol. Chem.* **2010**, *285*, 30170-80.

(6) Chen, W. Y.; Abatangelo, G. Functions of hyaluronan in wound repair. *Wound Repair Regen.* **1999**, *7*, 79-89.

(7) Koochekpour, S.; Pilkington, G. J.; Merzak, A. Hyaluronic acid/CD44H interaction induces cell detachment and stimulates migration and invasion of human glioma cells in vitro. *Int. J. Cancer* **1995**, *63*, 450-4.

(8) Mochizuki, S.; Vink, H.; Hiramatsu, O.; Kajita, T.; Shigeto, F.; Spaan, J. A.; Kajiya, F. Role of hyaluronic acid glycosaminoglycans in shear-induced endothelium-derived nitric oxide release. *Am. J. Physiol. Heart Circ. Physiol.* **2003**, *285*, H722-6.

(9) Baranova, N. S.; Nileback, E.; Haller, F. M.; Briggs, D. C.; Svedhem, S.; Day, A. J.; Richter, R. P. The inflammation-associated protein TSG-6 cross-links hyaluronan via hyaluronan-induced TSG-6 oligomers. *J. Biol. Chem.* **2011**, *286*, 25675-86.

(10) Attili, S.; Richter, R. P. Self-assembly and elasticity of hierarchical proteoglycan-hyaluronan brushes. *Soft Matter* **2013**, *9*, 10473-83.

(11) Hardingham, T. E.; Muir, H. The specific interaction of hyaluronic acid with cartilage proteoglycan. *Biochim. Biophys. Acta* **1972**, *279*, 401-5.

(12) Richter, R. P.; Baranova, N. S.; Day, A. J.; Kwok, J. C. Glycosaminoglycans in extracellular matrix organisation: are concepts from soft matter physics key to understanding the formation of perineuronal nets? *Curr. Opin. Struct. Biol.* **2018**, *50*, 65-74.

(13) Bourguignon, L. Y.; Lokeshwar, V. B.; Chen, X.; Kerrick, W. G. Hyaluronic acid-induced lymphocyte signal transduction and HA receptor (GP85/CD44)-cytoskeleton interaction. *J. Immunol.* **1993**, *151*, 6634-44.

(14) Fraser, S. P. Hyaluronan activates calcium-dependent chloride currents in Xenopus oocytes. *FEBS Lett.* **1997**, *404*, 56-60.

(15) Jessen, T. E.; Odum, L. TSG-6 and calcium ions are essential for the coupling of inter-alpha-trypsin inhibitor to hyaluronan in human synovial fluid. *Osteoarthritis Cartilage* **2004**, *12*, 142-8.

(16) Lenormand, H.; Vincent, J.-C. pH effects on the hyaluronan hydrolysis catalysed by hyaluronidase in the presence of proteins: Part II. The electrostatic hyaluronan – Protein complexes. *Carbohydr. Polym.* **2011**, *85*, 303-11.

(17) Zheng Shu, X.; Liu, Y.; Palumbo, F. S.; Luo, Y.; Prestwich, G. D. In situ crosslinkable hyaluronan hydrogels for tissue engineering. *Biomaterials* **2004**, *25*, 1339-48.
(18) Morra, M.; Cassineli, C. Non-fouling properties of polysaccharide-coated surfaces. *J. Biomater. Sci. Polym. Ed.* **1999**, *10*, 1107-24.
(19) Horkay, F.; Basser, P. J.; Londono, D. J.; Hecht, A. M.; Geissler, E. Ions in hyaluronic acid solutions. *J Chem Phys* **2009**, *131*, 184902.
(20) Buhler, E.; Boué, F. Chain persistence length and structure in hyaluronan solutions: Ionic strength dependence for a model semirigid polyelectrolyte. *Macromolecules* **2004**, *37*, 1600-10.
(21) Chakrabarti, B.; Balazs, E. A. Optical properties of hyaluronic acid: Ultraviolet circular dichroism and optical rotatory dispersion. *J. Mol. Biol.* **1973**, *78*, 135-41.
(22) Winter, W. T.; Arnott, S. Hyaluronic acid: the role of divalent cations in conformation and packing. *J. Mol. Biol.* **1977**, *117*, 761-84.
(23) Napier, M. A.; Hadler, N. M. Effect of calcium on structure and function of a hyaluronic acid matrix: carbon-13 nuclear magnetic resonance analysis and the diffusional behavior of small solutes. *Proc Natl Acad Sci U S A* **1978**, *75*, 2261-5.
(24) Carr, M. E.; Hadler, N. M. Permeability of hyaluronic acid solutions. *Arthritis Rheum.* **1980**, *23*, 1371-5.
(25) Gabriel, D. A.; Carr, M. E., Jr. Calcium destabilizes and causes conformational changes in hyaluronic acid. *Am. J. Med. Sci.* **1989**, *298*, 8-14.
(26) Gatej, I.; Popa, M.; Rinaudo, M. Role of the pH on hyaluronan behavior in aqueous solution. *Biomacromolecules* **2005**, *6*, 61-7.
(27) Maleki, A.; Kjøniksen, A. L.; Bo, N. Effect of pH on the behavior of hyaluronic acid in dilute and semidilute aqueous solutions. *Macromol. Symp.* **2008**, *274*, 131–40.
(28) Attili, S.; Richter, R. P. Combining colloidal probe atomic force and reflection interference contrast microscopy to study the compressive mechanics of hyaluronan brushes. *Langmuir* **2012**, *28*, 3206-16.
(29) Attili, S.; Borisov, O. V.; Richter, R. P. Films of end-grafted hyaluronan are a prototype of a brush of a strongly charged, semiflexible polyelectrolyte with intrinsic excluded volume. *Biomacromolecules* **2012**, *13*, 1466-77.
(30) Limozin, L.; Sengupta, K. Quantitative reflection interference contrast microscopy (RICM) in soft matter and cell adhesion. *ChemPhysChem* **2009**, *10*, 2752-68.
(31) Richter, R. P.; Hock, K. K.; Burkhartsmeyer, J.; Boehm, H.; Bingen, P.; Wang, G.; Steinmetz, N. F.; Evans, D. J.; Spatz, J. P. Membrane-grafted hyaluronan films: a well-defined model system of glycoconjugate cell coats. *J. Am. Chem. Soc.* **2007**, *129*, 5306-7.
(32) Schilling, J.; Sengupta, K.; Goennenwein, S.; Bausch, A. R.; Sackmann, E. Absolute interfacial distance measurements by dual-wavelength reflection interference contrast microscopy. *Phys. Rev. E Stat. Nonlin. Soft Matter Phys.* **2004**, *69*, 021901.
(33) Takahashi, R.; Al-Assaf, S.; Williams, P. A.; Kubota, K.; Okamoto, A.; Nishinari, K. Asymmetrical-Flow Field-Flow Fractionation with On-Line Multiangle Light Scattering Detection. 1. Application to Wormlike Chain Analysis of Weakly Stiff Polymer Chains. *Biomacromolecules* **2003**, *4*, 404-9.
(34) Pincus, P. Colloid stabilization with grafted polyelectrolytes. *Macromolecules* **1991**, *24*, 2912-9.
(35) Borisov, O. V.; Zhulina, E. B.; Birshtein, T. M. Diagram of the States of a Grafted Polyelectrolyte Layer. *Macromolecules* **1994**, *27*, 4795-803.

(36) Zhulina, E. B.; Klein Wolterink, J.; Borisov, O. V. Screening effects in a polyelectrolyte brush: self-consistent-field theory. *Macromolecules* **2000**, *33*, 4945-53.
(37) Ligoure, C.; Leibler, L. Thermodynamics and kinetics of grafting end-functionalized polymers to an interface. *J. Phys. (France)* **1990**, *51*, 1313-28.
(38) Israelachvili, J. N. In *Intermolecular and Surface Forces (Third Edition)*; Academic Press: San Diego, 2011291-340.
(39) Reviakine, I.; Johannsmann, D.; Richter, R. P. Hearing what you cannot see and visualizing what you hear: interpreting quartz crystal microbalance data from solvated interfaces. *Anal. Chem.* **2011**, *83*, 8838-48.
(40) Mohan, C., *Buffers. A guide for the preparation and use of buffers in biological systems*. 2006: EMD Bioscience
(41) Borisov, O. V.; Zhulina, Y. B.; Birshtein, T. M. Constitutional diagram and collapse of grafted chain layers. *Polym. Sci. (USSR)* **1988**, *30*, 772-9.
(42) Zhulina, E. B.; Birshtein, T. M.; Priamitsyn, V. A.; Klushin, L. I. Inhomogeneous Structure of Collapsed Polymer Brushes Under Deformation. *Macromolecules* **1995**, *28*, 8612-20.
(43) Eisele, N. B.; Labokha, A. A.; Frey, S.; Gorlich, D.; Richter, R. P. Cohesiveness tunes assembly and morphology of FG nucleoporin domain meshworks - Implications for nuclear pore permeability. *Biophys. J.* **2013**, *105*, 1860-70.
(44) Gura, E.; Hückel, M.; Müller, P. J. Specific degradation of hyaluronic acid and its rheological properties. *Polym. Degradation Stab.* **1998**, *59*, 297-302.
(45) Sivasankar, S.; Subramaniam, S.; Leckband, D. Direct molecular level measurements of the electrostatic properties of a protein surface. *Proc. Natl. Acad. Sci. U. S. A.* **1998**, *95*, 12961-6.
(46) Balazs, E. A.; Cui, J. The story of "Hyaluronan putty". *Bioact. Carbohydr. Dietary Fibre* **2013**, *2*, 143-51.
(47) Wu, S.; Ai, L.; Chen, J.; Kang, J.; Cui, S. W. Study of the mechanism of formation of hyaluronan putty at pH 2.5: Part II—Theoretical analysis. *Carbohydr. Polym.* **2013**, *98*, 1683-8.
(48) Zhulina, E. B.; Israels, R.; Fleer, G. J. Theory of planar polyelectrolyte brush immersed in solution of asymmetric salt. *Colloids Surf. A: Physicochem. Eng. Asp.* **1994**, *86*, 11-24.
(49) Zhulina, E. In *Solvents and Self-Organization of Polymers*; Webber, S. E., Munk, P.,Tuzar, Z., Eds.; Springer Netherlands: Dordrecht, 1996227-58.
(50) Winter, W. T.; Arnott, S. Hyaluronic acid: the role of divalent cations in conformation and packing. *J. Mol. Biol.* **1977**, *117*, 761-84.
(51) Manning, G. S. Limiting Laws and Counterion Condensation in Polyelectrolyte Solutions. I. Colligative Properties. *The Journal of Chemical Physics* **1969**, *11*, 924-33.
(52) Gribbon, P.; Heng, B. C.; Hardingham, T. E. The analysis of intermolecular interactions in concentrated hyaluronan solutions suggest no evidence for chain-chain association. *Biochem. J.* **2000**, *350*, 329-35.
(53) Bano, F.; Banerji, S.; Howarth, M.; Jackson, D. G.; Richter, R. P. A single molecule assay to probe monovalent and multivalent bonds between hyaluronan and its key leukocyte receptor CD44 under force. *Sci Rep* **2016**, *6*, 34176.
(54) Robertson, W. G. Measurement of ionized calcium in biological fluids. *Clinica chimica acta; international journal of clinical chemistry* **1969**, *24*, 149-57.

(55) Burger, K.; Illes, J.; Gyurcsik, B.; Gazdag, M.; Forrai, E.; Dekany, I.; Mihalyfi, K. Metal ion coordination of macromolecular bioligands: formation of zinc(II) complex of hyaluronic acid. *Carbohydr Res* **2001**, *332*, 197-207.
(56) Soltes, L.; Stankovska, M.; Brezova, V.; Schiller, J.; Arnhold, J.; Kogan, G.; Gemeiner, P. Hyaluronan degradation by copper(II) chloride and ascorbate: rotational viscometric, EPR spin-trapping, and MALDI-TOF mass spectrometric investigations. *Carbohydr Res* **2006**, *341*, 2826-34.
(57) Rubinstein, M.; Colby, R. H., *Polymer physics*. 2003, Oxford ; New York: Oxford University Press. xi, 440 p.
(58) de Gennes, P. G., *Scaling concepts in polymer physics*. 1979, Ithaca, N.Y.: Cornell University Press. 324 p.

SUPPLEMENTARY MATERIAL

Effect of calcium ions and pH on the morphology and mechanical properties of hyaluronan brushes

Xinyue Chen and Ralf P. Richter*

** Corresponding author: email: r.richter@leeds.ac.uk*

TABLE OF CONTENTS

SUPPLEMENTARY METHODS

Refinement of the colloidal probe RICM analysis for coated glass substrates

In previous work,[1] we found an algorithm that is based on the quantification of the radial position of intensity extrema in colloidal probe interferographs[1,2] to work well for quantifying the thickness of HA brushes formed on bare glass. In the present work, HA brushes were formed on glass that was coated with a thin metal film. In the following, we show that the established method can also be applied on metal-coated glass with a simple modification.

We follow textbook knowledge[3] to describe the interference of light following transmission and reflection at multiple interfaces (Fig. S1*A*). For two parallel interfaces – formed by medium 0, an interlayer of medium 1, and medium 2 – the total reflectance R, which determines the reflected intensity $I_{\text{reflection}}$ for a given intensity $I_{\text{incidence}}$ of the incident light, is given by

$$R = I_{\text{reflection}} / I_{\text{incidence}} = |r_{012}|^2, \qquad \text{(Eq. 1)}$$

where r_{012} presents the total effective reflection coefficient. This coefficient takes all light beams reflected back into medium 0 into account (Fig. S1*A*) and is given by

$$\begin{aligned} r_{012} &= r_{01} + t_{01}t_{10}r_{12}e^{-i2\beta} + t_{01}t_{10}r_{10}r_{12}e^{-i4\beta} + t_{01}t_{10}r_{10}{}^2r_{12}e^{-i6\beta} + \cdots, \\ &= r_{01} + [r_{01} + r_{12}\exp(-i2\beta)]/[1 + r_{01}r_{12}\exp(-i2\beta)] \end{aligned} \qquad \text{(Eq. 2)}$$

where r_{xy} and t_{xy} are the local reflection and transmission coefficients at the interface between media x and y. The phase variation between two contiguous outcoming beams is constant. Assuming to a first approximation that light is incident perpendicular to the substrate, it is expressed as

$$\beta = 2\pi\tilde{n}_1 d / \lambda, \qquad \text{(Eq. 3)}$$

where $\tilde{n}_1$ and d are the complex refractive index and the thickness of the interlayer, and λ is the wavelength of the incident light. Both reflection and transmission coefficients are then easily determined as

$$r_{xy} = (\tilde{n}_x - \tilde{n}_y)/(\tilde{n}_x + \tilde{n}_y) \text{ and } t_{xy} = 1 - r_{xy}. \qquad \text{(Eq. 4)}$$

The complex refractive index, expressed as

$$\tilde{n} = n - i \cdot 2\pi k / \lambda, \qquad \text{(Eq. 5)}$$

considers the refractive index n and the extinction coefficient k, and thus is appropriate for fully transparent layers (such as glass or the solution) as well as light-absorbing layers (such as Au).

The case of two interlayers can be reduced to the case of one interlayer (Fig. S1*B*), that is, the effective reflection coefficient r_{123} of a system consisting of media 1, 2 and 3 can first be determined by the approach described above, and then integrated with medium 0 by treating the two interlayers (made of media 1 and 2) as a single layer with effective optical properties. The total effective reflection coefficient is then

$$r_{0123} = r_{01} + [r_{01} + r_{123}\exp(-i2\beta)]/[1 + r_{01}r_{123}\exp(-i2\beta)]. \qquad \text{(Eq. 6)}$$

This method can be further expanded for more interlayers.

To reproduce our experimental setup, we simulated the reflectance of a system consisting of a glass substrate, followed by a metal film (0.5 nm Ti adhesion layer + 5 nm Au), a hydrated organic film (8 nm, representing the OEG and SAv monolayers), a buffer layer of variable thickness (representing the space between the planar coated substrate and a given position on the surface of the colloidal probe; due to its strong hydration, the refractive index of the HA film can be considered equivalent to that of buffer to a good approximation) and a polystyrene medium (representing the colloidal probe). The optical properties used for the different media are provided in Table S1 and the results are shown in Fig. S1*C*.

The data in Fig. S1*C* illustrate the periodic dependence of the reflectivity on the probe-substrate distance. Importantly, the sinusoidal shape of the curve is not appreciably distorted by the metal film, alone (*red curve*) or in conjunction with the organic film (*blue curve)*, as compared to the bare glass (*black curve*), and the length of the period (λ / 2 n_{buffer}) also remains unchanged. The position of the extrema, on the other hand, is sensibly affected.

Table S1. Refractive indices and extinction coefficients used in the simulation of reflectance.

	Glass	Ti	Au	Organic film	Buffer	Polystyrene
n	1.514	1.771	1.017	1.450	1.333	1.550
k	0	2.374	1.826	0	0	0

These theoretical predictions justify our approach to analyze the experimental RICM data. Specifically, we used the analysis approach previously established for bare glass[1] to determine (i) the effective probe-surface distance H_{ref} on a reference surface featuring the metal film, the OEG monolayer and the SAv monolayer, and (ii) the effective probe-surface distance H_{HA} on an identically prepared surface with grafted HA. The real probe-substrate distance was then obtained as $H = H_{HA} - H_{ref}$. The offset by H_{ref} fully accounts for the effect of the metal and organic films on the position of the extrema with respect to the probe-surface separation.

We note in passing that Fig. S1*C* also shows that the maximal reflectance is enhanced with the metal film. This was indeed observed in the experiment and is an advantage as it enhances image contrast.

SUPPLEMENTARY FIGURES

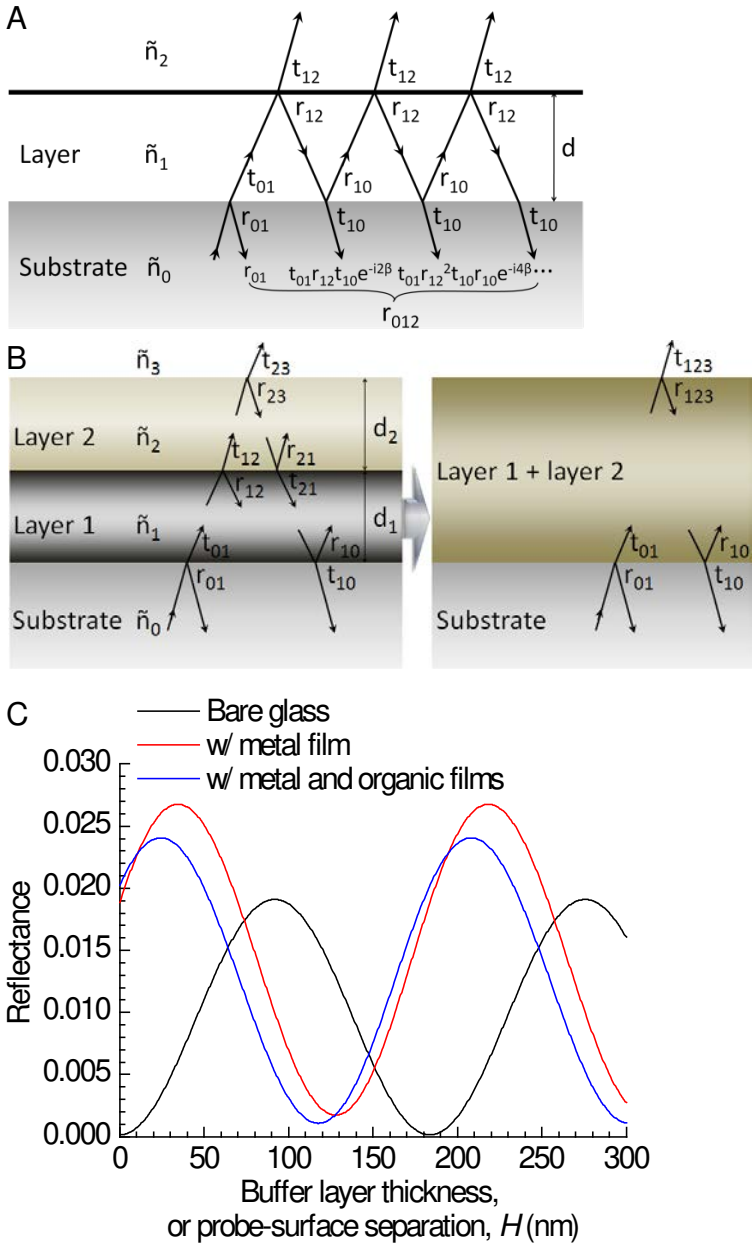

Figure S1. Impact of coatings on the glass substrate on RICM data analysis. (*A*) Schematic of the multiple reflections occurring at a single layer (medium 1) sandwiched between two other media (0 and 2). (*B*) Schematic of the light paths in a system with two layers and simplification to a single effective layer. (*C*) Simulated reflectance for a multilayer system consisting of a glass substrate, a buffer interlayer and polystyrene as a function of the buffer interlayer thickness *H* (for details see the text above and Table S1; λ= 490 nm). The glass was either bare (*black curve*), coated with a metal film (*red curve*), or coated with a metal film and an organic film (*blue curve*). In the experiment, the data would correspond to the reflectance at the centre of the colloidal probe as a function of the probe-surface separation *H*.

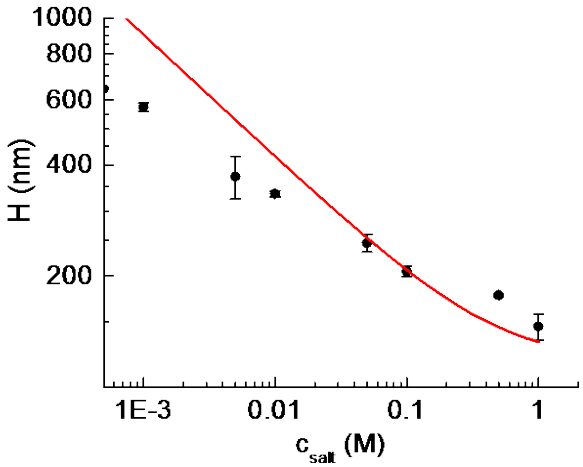

Figure S2. Estimation of grafting density. Unperturbed HA brush thickness measured at different NaCl concentration (*symbols*, extracted from Fig. 2) together with a fit (*line*, to data ≥ 50 mM NaCl) with a previously developed mean field theory.[4] From the fit, a root-mean-square distance $s = 51$ nm between anchor points is estimated.

The mean field approach treats HA as a semi-flexible polymer and the electrostatic repulsion between polyelectrolyte chains in the brush as an effective excluded volume, and has previously been found to describe HA brushes in NaCl solutions of sufficiently high ionic strength (≥ 50 mM) well.[4] Specifically, the thickness is predicted to depend on ionic strength as $H = (8/\pi^2)^{1/3} (pv/bs^2)^{1/3} l_c$, where l_c is the polymer contour length, b the monomer unit length, p characterizes the intrinsic chain stiffness, and v is the effective excluded volume. At high ionic strength, $v = v_0 + \alpha^2 / (4c_{NaCl})$, where α is the fractional charge per monomer unit and $v_0 = Ab^3$ the 'bare' excluded volume in the absence of charge repulsion (A is a numerical pre-factor, and depends on the monomer shape and the solvent quality). For the fitting, we used $p = 14$, $b = 1$ nm, $A = 0.9$ and $\alpha = 1$ (as established in ref. 4), $l_c = 740$ nm (equivalent to 280 kDa HA), and s was the only adjustable parameter.

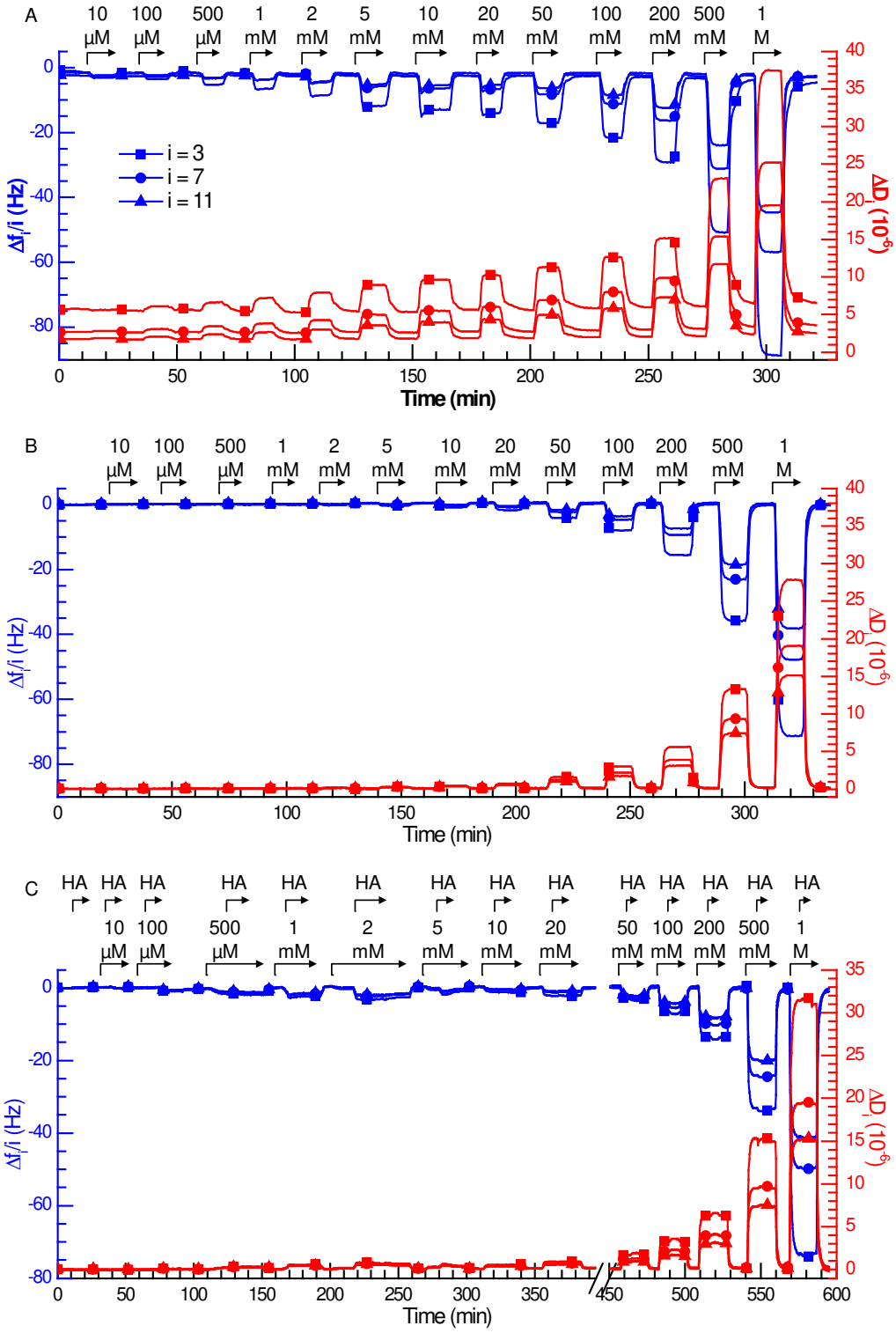

Figure S3. Effect of calcium ions on HA brushes, characterized by QCM-D. Representative time-resolved data for an HA brush (prepared as in Fig. 1*B*; *A*), a reference surface (SAv monolayer without HA; *B*), and non-specific binding of non-biotinylated HA to the reference surface (*C*). Shifts in normalized frequency, $\Delta f_i/i$, and in dissipation, ΔD_i, relative to a SAv monolayer in ultrapure water are displayed for overtones $i = 3$, 7 and 11 (as indicated in *A*). The start and duration of incubation of $CaCl_2$ (at various concentrations, as displayed) or HA (at 10 µg/mL) are indicated by arrows on top; during remaining times, surfaces were exposed to ultrapure water. The QCM-D responses upon incubation of $CaCl_2$ solution in *B* do not reflect any changes on the surface but result from changes in viscosity and/or density of the solution owing to the added $CaCl_2$. The frequency and dissipation shifts displayed in Fig. 3*A*-*B* were obtained by subtracting data in *B* from *A*, and essentially reflect the HA film alone.

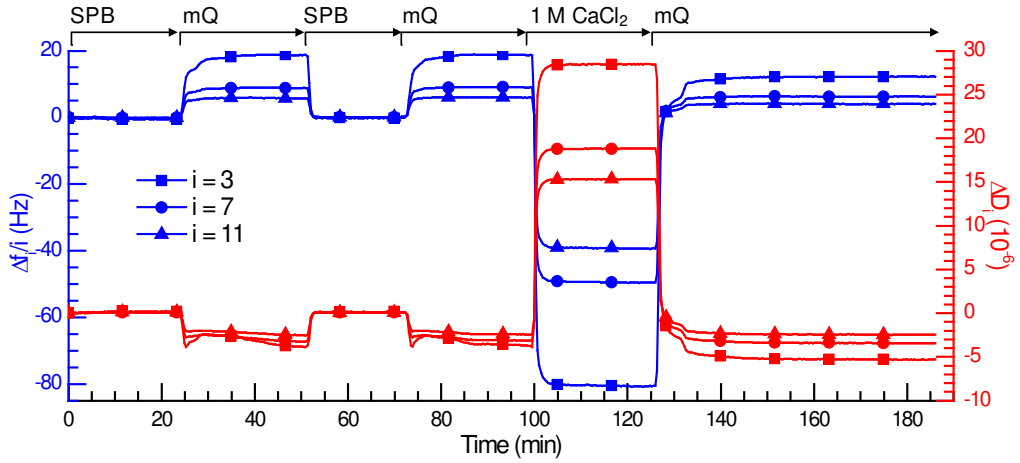

Figure S4. Reversibility of calcium effect on HA brushes. An HA brush was prepared as in Fig. 1*B*, and time-resolved QCM-D data at overtones i = 3, 7 and 11 for the response to various solutions (indicated by arrows on top) are shown. The transition from sample preparation buffer (SPB) to ultrapure water (mQ) is fully reversible, but 1 M $CaCl_2$ in ultrapure water has a minor irreversible effect on the HA brush.

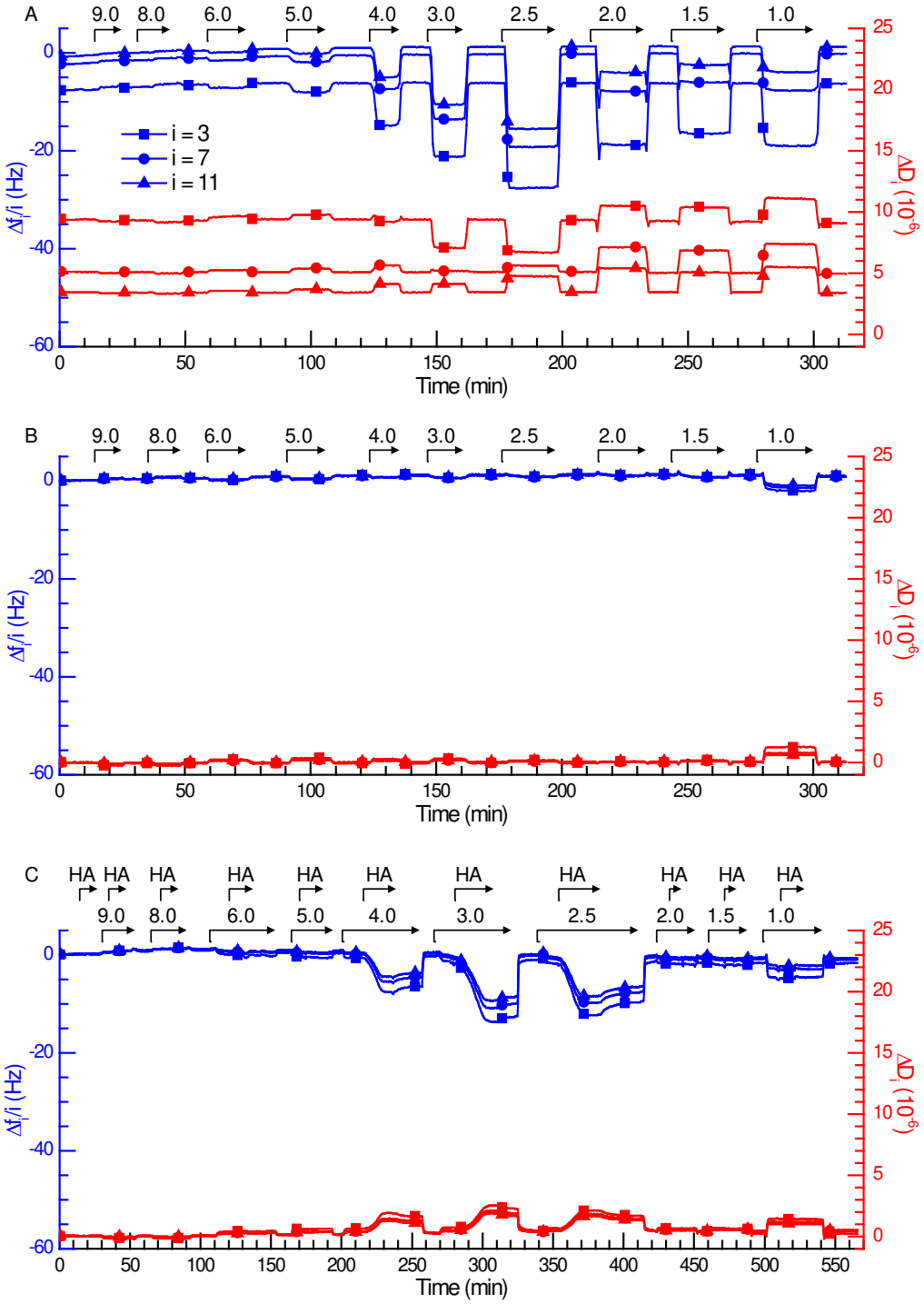

Figure S5. Effect of pH on HA brushes, characterized by QCM-D. Representative time-resolved data for an HA brush (prepared as in Fig. 1*B*; *A*), a reference surface (SAv monolayer without HA; *B*), and non-specific binding of non-biotinylated HA to the reference surface (*C*). Overtones i = 3, 7 and 11 are shown, as indicated in *A*. The start and duration of incubation of potassium phosphate buffer (containing 100 mM potassium ions at various pH, as displayed) or HA (at 10 µg/mL) are indicated by arrows on top; during remaining times, surfaces were exposed to potassium phosphate buffer at pH 7.0. The QCM-D responses upon incubation of solutions with different pH in *B* do not reflect any changes on the surface but result from changes in viscosity and/or density of the solution owing to the presence of added salt. The frequency and dissipation shifts displayed in Fig. 5*A*-*B* were obtained by subtracting data in *B* from *A*, and essentially reflect the HA film alone.

SUPPLEMENTARY REFERENCES

1. Attili, S.; Richter, R. P. Combining colloidal probe atomic force and reflection interference contrast microscopy to study the compressive mechanics of hyaluronan brushes. *Langmuir* **2012,** *28*, 3206-16.
2. Limozin, L.; Sengupta, K. Quantitative reflection interference contrast microscopy (RICM) in soft matter and cell adhesion. *ChemPhysChem* **2009,** *10*, 2752-68.
3. Fujiwara, H. Principles of optics. In *Spectroscopic Ellipsometry*; John Wiley & Sons, Ltd, 2007, pp 13-48.
4. Attili, S.; Borisov, O. V.; Richter, R. P. Films of end-grafted hyaluronan are a prototype of a brush of a strongly charged, semiflexible polyelectrolyte with intrinsic excluded volume. *Biomacromolecules* **2012,** *13*, 1466-77.